Modeling the Fracture of a Sandwich Structure due to Cavitation in a Ductile Adhesive Layer

S. Zhang

K. J. Hsia[1]
Mem. ASME,

Department of Theoretical
and Applied Mechanics,
University of Illinois at Urbana-Champaign,
Urbana, IL 61801

The strength and durability of adhesively bonded sandwich structures often depend on the mechanisms of fracture, which in turn depend on the properties of the adhesive and the microstructures of the interface. When the thin adhesive layer is ductile, cavitation either within the layer or along the interface is often the dominant failure mechanism. In the present paper, fracture due to cavity growth in a thin ductile layer is analyzed. A new method utilizing fluid mechanics solutions is developed. Solutions of fluid flow field are used to approximate the plastic deformation field in the corresponding solid body with a cavity. The equilibrium condition is satisfied by using the principle of virtual work rate. Stress-separation curves due to cavitation in the thin layer can thus be obtained. The method is validated by reevaluating the one-dimensional problem of cavity growth in a sphere—a problem for which an exact, analytical solution exists. A two-dimensional plane strain cavitation problem is analyzed using the new method. The stress-separation curves and the fracture resistance due to this mechanism are obtained. The results show that both the stress-separation curves and the fracture resistance are sensitive to the strain-hardening exponent and the initial void size, but not the yield strength of the material. The new method has clear advantages over numerical methods, such as the finite element method, when parametric studies are performed.
[DOI: 10.1115/1.1346678]

1 Introduction

The strength and durability of sandwich structures consisting of two ceramic or metal pieces bonded by a thin adhesive layer are determined by various failure mechanisms. These fracture mechanisms include interfacial debonding and other processes such as cavitation or microcracking within the adhesive layer or at the interface. Identifying and understanding the failure mechanisms in these structures will greatly enhance our ability to design better, more durable structures.

The failure mechanisms, however, are ultimately determined by the properties of the adhesive and by the microstructures of the interface in sandwich structures. The current research stems from the need to tailor the surface microstructures of aluminum panels by surface treatments in preparation for adhesive bonding (see, e.g., [1,2]). Within the constraints of surface treatment technology, a guideline to achieve an optimized microstructure is highly desirable.

In many such structures, the adhesive is often a soft or ductile phase. It may be a polymer-based material for joints in aircraft structures, or ductile metal in metal/ceramic composites. There have been many studies on failure mechanisms within a ductile layer bonding two substrate pieces together ([3–7]). When the adhesive layer is sufficiently soft, the failure process is crack propagation by void growth and coalescence within the ductile layer or along the interface. In this case, a large hydrostatic stress is developed in the ductile layer due to the constraint on plastic flow by the substrate, leading to void nucleation ahead of the crack tip. The location and density of void nucleation, however, is often related to the microstructures of the interface, such as initial pore density and interface roughness. For given microstructures, the initial void density can be considered as given. Failure of such sandwich structures is then directly related to the microstructures of the interface.

Fracture process of a material can be characterized by the stress-separation curve ahead of the crack tip. For purely brittle fracture of crystals, such stress-separation curves can be derived from the interatomic potentials. When nonlinear processes are involved, however, derivations of such stress-separation curves must invoke micromechanisms during fracture. For example, plastic dissipation must be taken into account in the case of elastoplastic fracture. Analyses of crack growth resistance due to plastic dissipation were carried out by Tvergaard and Hutchinson [8,9], who identified several dimensionless groups of material parameters characterizing the fracture process. An equivalent stress-separation curve for fracture due to cavity growth and coalescence may be derived from the detailed study of the cavitation process. In the present paper, failure due to cavity growth and coalescence will be studied by analyzing the stress-separation curves during cavity growth.

Cavitation has been studied by many researchers since the 1960s. The pioneer work by McClintock [10] revealed that the volume expansion rate of a long cylindrical cavity in a nonhardening material subjected to transverse tensile stress increases exponentially with the transverse stress. Rice and Tracey [11] analyzed the growth of a single spherical void embedded in an infinite body subjected to remote uniform tensile stresses. They found that the ratio of void growth rate to remote strain rate increases exponentially as the ratio of mean normal stress to yield stress increases. Their analysis also predicted that void growth is mainly due to volume change rather than shape change of the void when the remote normal stress is large. Both the above analyses were carried out on an infinite body, which is inappropriate for cavities in a confined ductile layer. Needleman [12] and Andersson [13] studied void growth numerically in a finite body using

[1]To whom correspondence should be addressed.

Contributed by the Applied Mechanics Division of THE AMERICAN SOCIETY OF MECHANICAL ENGINEERS for publication in the ASME JOURNAL OF APPLIED MECHANICS. Manuscript received by the ASME Applied Mechanics Division, Oct. 1, 1999; final revision, July 19, 2000. Associate Editor: B. Moran. Discussion on the paper should be addressed to the Editor, Professor Lewis T. Wheeler, Department of Mechanical Engineering, University of Houston, Houston, TX 77204-4792, and will be accepted until four months after final publication of the paper itself in the ASME JOURNAL OF APPLIED MECHANICS.

the finite element method. In these studies the interaction between voids was taken into account, but the amount of cavity growth was limited. More recently Tvergaard [14] analyzed void growth in a thin, ductile layer between ceramics using finite element method, and employed a remeshing technique for the final stage of growth. These numerical studies require tremendous computing power, and are usually rather time-consuming.

If the material of the ductile layer obeys an elastoplastic constitutive law, the nonlinearity of the governing equations seems to exclude the possibility of obtaining exact solutions for all but the one-dimensional case studied by McClintock [10] and Huang et al. [15]. In the present paper, to derive the stress-separation curves for a material undergoing cavitation in a thin ductile layer, we develop a novel approach to finding an admissible deformation field around the void. The approach utilizes fluid mechanics solutions of a point source in a finite unit cell, and approximates the plastic deformation field with a fluid flow field. The appropriateness of the approach is verified by reevaluating the spherically symmetric cavitation problem for which an analytical solution exists ([10,15]). A two-dimensional plane strain problem is then analyzed to obtain the stress-separation relation of a unit cell with a center cavity. The results show that the stress-separation relations depend not only on the material properties but also on the geometrical parameters (microstructures), such as initial void size and void spacing.

2 Spherically Symmetric Cavitation

We begin our discussion by considering the spherically symmetric cavitation problem. Consider a spherical void centered in an isotropic, rigid-plastic sphere (either perfectly plastic or strain hardening without elastic response) subjected to hydrostatic tension σ_s (see Fig. 1). A uniaxial relation between the true stress, σ, and the logarithmic strain, ε, of the solid is given by

$$\sigma/\sigma_Y = f(\varepsilon) = \left|\frac{E}{\sigma_Y}\varepsilon\right|^N \mathrm{sgn}(\varepsilon) \tag{1}$$

where σ_Y is the tensile yield strength of the solid, E is the Young's Modulus, N is the hardening exponent ($0 \leqslant N \leqslant 1$), $\mathrm{sgn}(\varepsilon)$ represents the sign of ε. The limit $N=0$ corresponds to a rigid-perfectly plastic material.

Two different methods to obtain the relation between the hydrostatic stress and the void expansion are presented. One method is based on classical plasticity theory in solid mechanics. The other employs a fluid mechanics approach, and treats the void as a point source of material flowing outward under the applied stress. With the latter the plastic deformation is to be represented by a potential flow generated from a point source. Both methods are capable of solving this one-dimensional cavitation problem analytically, as shown below.

2.1 Solid Mechanics Method. In what follows, capital letters stand for variables in the initial configuration and lowercase ones stand for variables in the current, deformed configuration. Let R_0 and r_0 be the radii of the cavity in the initial and current configuration, and R_1 and r_1 be the radii of the outer boundary in the initial and current state, respectively (Fig. 1). By symmetry, the true strain components in spherical coordinates (r,θ,φ) are

$$\varepsilon_\theta = \varepsilon_\varphi = -\frac{1}{2}\varepsilon_r = -\ln\frac{r}{R} \tag{2a}$$

$$\varepsilon_e = 2\ln\left(\frac{r}{R}\right) = \varepsilon_r \tag{2b}$$

where ε_e is the von Mises equivalent strain, defined as

$$\varepsilon_e = \sqrt{\frac{2}{3}\varepsilon_{ij}\varepsilon_{ij}} \tag{3}$$

where ε_{ij} $(i,j=r,\theta,\varphi)$ are the logarithmic strain components, and the summation convention applies in Eq. (3). The equilibrium condition in terms of radial stress σ_r and hoop stress σ_θ in the current configuration is

$$\frac{d\sigma_r}{dr} + \frac{2}{r}(\sigma_r - \sigma_\theta) = 0. \tag{4}$$

The von Mises equivalent stress in the spherically symmetric case can be expressed as

$$\sigma_e = \sigma_r - \sigma_\theta. \tag{5}$$

Assuming that the material obeys J_2-deformation theory, i.e., the relation between equivalent stress and equivalent strain follows that of uniaxial relation in Eq. (1), one has

$$\frac{\sigma_r - \sigma_\theta}{\sigma_Y} = f(\varepsilon_r) \tag{6}$$

where the function $f(\varepsilon_r)$ is given in Eq. (1). Using the boundary conditions $(\sigma_r|_{r=r_0}=0, \sigma_r|_{r=r_1}=\sigma_s)$ and the incompressibility requirement $(r^3 - r_0^3 = R^3 - R_0^3)$, and substituting Eqs. (2) and (6) into Eq. (4), one finds

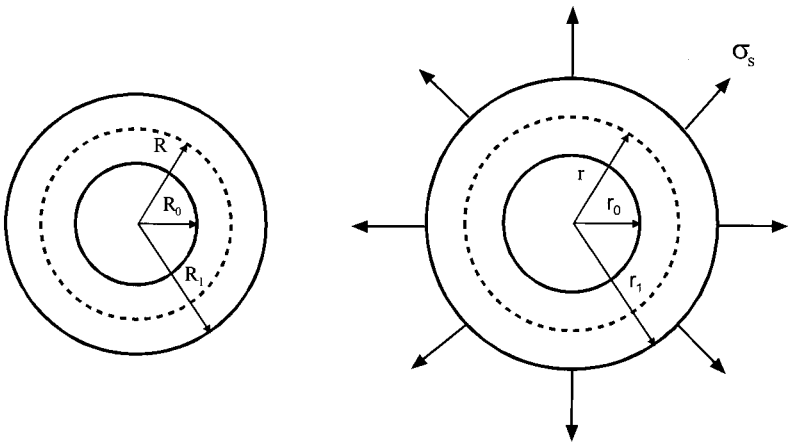

Fig. 1 Geometry of the spherically symmetric void in the initial and deformed states

$$\frac{\sigma_s(r_0)}{\sigma_Y}=-2\int_{R_0}^{R_1}\frac{R^2}{R^2+r_0^3-R_0^3}f\left\{-\frac{2}{3}\ln\left(1+\frac{r_0^3-R_0^3}{R^3}\right)\right\}dR. \tag{7}$$

Equation (7) gives the relationship between the applied hydrostatic stress and the cavity radius, $\sigma_s(r_0)$. It should be pointed out that the solution in Eq. (7) is identical to that obtained by Huang et al. [15].

2.2 Fluid Mechanics Method. The problem shown in Fig. 1 can also be solved using a fluid mechanics approach. Consider a potential flow generated by a point source of strength Q at the center of the sphere. The velocity components of the potential flow in spherical coordinates (r,θ,φ) are given by

$$\dot{u}_r=\frac{Q}{4\pi r^2},\quad \dot{u}_\theta=\dot{u}_\varphi=0. \tag{8}$$

Integrating the radial velocity with respect to time with the initial condition $r|_{t=0}=R$ gives

$$Qt=\frac{4\pi}{3}(r^3-R^3). \tag{9}$$

This equation shows that r^3-R^3 is an invariant throughout the solid body at any specific time t. This invariance requirement implies incompressibility of the material.

The strain rate components can be obtained from the velocity components by taking the derivative of the radial velocity with respect to the radius r, or by dividing the radial velocity by r, as

$$\dot{\varepsilon}_r=-\dot{\varepsilon}_e=-2\dot{\varepsilon}_\theta=-2\dot{\varepsilon}_\varphi=-\frac{Q}{2\pi r^3} \tag{10}$$

where $\dot{\varepsilon}_e$ is the equivalent strain rate defined as

$$\dot{\varepsilon}_e=\sqrt{\frac{2}{3}\dot{\varepsilon}_{ij}\dot{\varepsilon}_{ij}} \tag{11}$$

where $\dot{\varepsilon}_{ij}$ $(i,j=r,\theta,\varphi)$ are the true strain rate components. By integrating the strain rates with respect to time and using the incompressibility condition, one finds exactly the same expression as in Eq. (2). This result shows that the potential flow generated by a point source gives the same plastic deformation field around the void as that by the solid mechanics method given in Section 2.1.

To obtain the stress-cavity growth relations, we use here the principle of virtual work rate instead of the equilibrium equation in solid mechanics. Such an approach is entirely based on the estimates of the velocity field and strain rate field, and makes use of the constitutive law in an integral sense. The principle of virtual work rate in the current state is

$$\int_S\sigma_s\dot{u}_r dS=\int_V\sigma_{ij}\dot{\varepsilon}_{ij}dV \tag{12}$$

where S is the surface (including the outer surface and the inner surface although the work done on the inner surface is zero since it is traction-free) and V is the volume of the solid. Assuming again that the material follows the J_2 flow rule and it is a von Mises material, one has

$$s_{ij}=\frac{2}{3}\frac{\sigma_e}{\dot{\varepsilon}_e}\dot{\varepsilon}_{ij} \tag{13}$$

where s_{ij} $(i,j=r,\theta,\varphi)$ represent the deviatoric stress components defined as

$$s_{ij}=\sigma_{ij}-\frac{1}{3}\sigma_{kk}\delta_{ij} \tag{14}$$

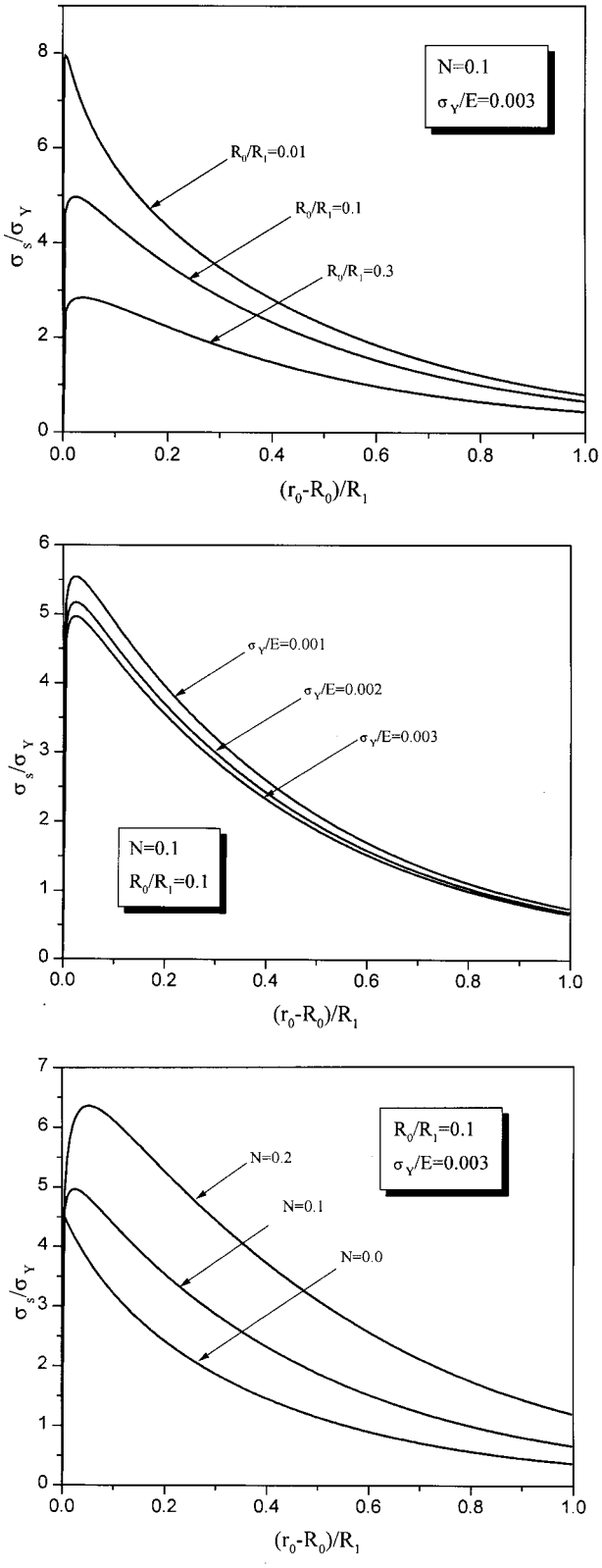

Fig. 2 Stress versus void radius for the growth of a spherically symmetrical void; (*a*) effects of the initial radius of cavity, (*b*) effects of the material constant σ_Y/E, (*c*) effects of the strain hardening exponent *N*

where $\sigma_{kk}=\sigma_{rr}+\sigma_{\theta\theta}+\sigma_{\varphi\varphi}$, and δ_{ij} is the Kronecker delta. Assuming that the constitutive law between the equivalent true stress and true strain follows the uniaxial relation expressed in Eq. (1), and using the flow field given in Eqs. (8), (10), and (11), one can rewrite Eq. (12) as

$$\frac{\sigma_s}{\sigma_Y}=\frac{1}{2\pi}\int_V f[2\ln(r/R)]r^{-3}dV. \tag{15}$$

Changing the variables to those for the initial state by using the incompressibility condition, one finally obtains the same stress-separation relationship as that in Eq. (7).

Using either Eq. (15) or Eq. (7), curves of the hydrostatic stress versus cavity radius are plotted in Figs. 2(*a*)–(*c*). Figure 2(*a*) shows the normalized hydrostatic stress versus the normalized current radius of the void for prescribed strain-hardening exponent and material constants σ_Y/E. Curves for three different values of initial void radius are plotted. The figure shows that the normalized stress reaches a maximum value rapidly, then decays monotonically as the cavity grows. The solution also shows that a smaller initial void size gives rise to a higher hydrostatic stress for a given amount of void growth and a higher maximum stress. When the loading process is stress-controlled, reaching the maximum load results in instability of void growth ([3,16–18]). When the loading is displacement-controlled, a softening stage (load drop) is experienced.

The effects of strain hardening exponent and yield strength on the stress versus void growth behavior are shown in Figs. 2(*b*)–(*c*). Figure 2(*b*) shows the normalized hydrostatic stress versus normalized void radius for different values of the material constant σ_Y/E for given initial radius of the cavity and strain-hardening exponent. Figure 2(*c*) shows the normalized stress versus normalized void radius for different values of strain-hardening exponent for given initial radius of the void and material constants. The figures show that the stress versus cavity growth curves are insensitive to the value of the normalized yield strength σ_Y/E, but rather sensitive to the strain-hardening exponent and the initial radius of the void. It is not unexpected to see strong dependence of the curves on hardening exponent and weak dependence on initial yield strength since the deformation becomes very large around the void as it grows. But the prediction of strong dependence on the initial cavity size is interesting.

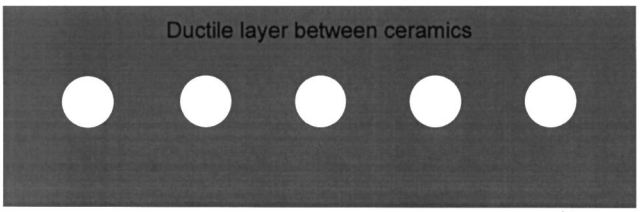

Fig. 3 Schematics of a cavitated ductile interface layer with periodic cavity distribution

3 Fully Confined Two-Dimensional Void Growth in a Thin Ductile Layer

In the previous section we showed that the method of using a fluid mechanics solution to approximate the plastic flow field is indeed a viable one. For the one-dimensional problem considered in the previous section, the solution turns out to be exact. But for more complicated cases, the solution can only be considered approximate. In the present section, we consider a two-dimensional problem.

A periodic array of cavities in a ductile layer fully confined by the interfaces, shown schematically in Fig. 3, is considered. Plane strain deformation is assumed. The cavities can be either completely within the ductile layer generated at, e.g., second phase particles, or at the interface generated from the interfacial pores. Due to symmetry of the problem, the solution should be identical for these two cases. The stress-separation curves, $\sigma(\delta)$, due to cavity growth and coalescence can be evaluated by considering a representative unit cell containing a single cavity. It is expected that, because of the confinement, plastic flow-induced cavity growth may start before the strength of the interface is reached. Due to the constraint by the rigid interface, high triaxial stresses will develop in the thin layer and will be the main driving force for cavity growth.

The geometry of the unit cell is presented in Fig. 4. The void spacing is $2w_0$, the layer thickness is $2h_0$, and the initial radius of the void is R_0. A Cartesian coordinate system with origin at the center of the cavity is established as in Fig. 4. Uniform tensile stress, σ_s, is applied normal to the thin layer. The periodicity condition requires that the width of the unit cell, $2w_0$, remains constant during deformation. The separation displacement, δ, is evaluated at the interface, $x=\pm h_0$.

To obtain the approximate plastic deformation field in the unit cell, we now consider a potential flow generated by a source of strength Q located at $z=0$ in an infinite channel in the domain $-w_0<y<w_0$ and $-\infty<x<\infty$; here $z=x+yi$ is the complex variable. The complex potential ψ of the flow field is found by conformal mapping, as

$$\psi(z)=\frac{Q}{2\pi}\ln\left\{\sinh\left(\frac{\pi z}{2w_0}\right)\right\}. \tag{16}$$

The velocity field corresponding to the potential flow is

$$\dot{u}_x-\dot{u}_y i=\frac{Q}{4w_0}\coth\left(\frac{\pi z}{2w_0}\right). \tag{17}$$

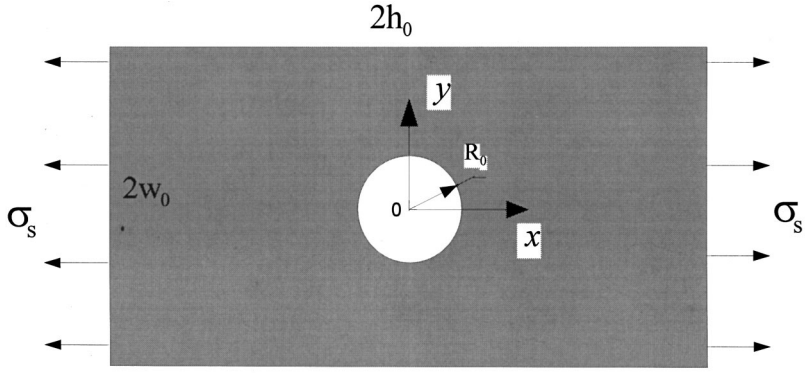

Fig. 4 Unit cell model used in the two-dimensional void growth analysis

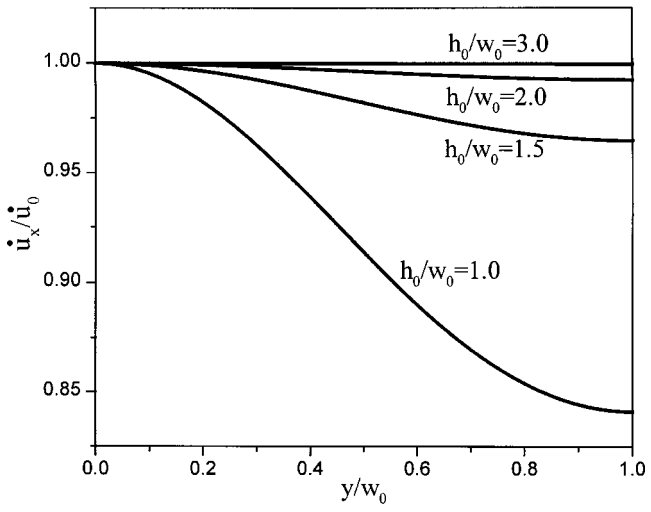

Fig. 5 Uniformity of the velocity field at the interface $x=h_0$

The Cauchy strain rates corresponding to the velocity field can be obtained by differentiating Eq. (17), as

$$\dot{\varepsilon}_{xx}-\dot{\varepsilon}_{xy}i=-\frac{\pi Q}{8w_0^2}\mathrm{csch}^2\left(\frac{\pi z}{2w_0}\right)$$
$$\dot{\varepsilon}_{xy}-\dot{\varepsilon}_{yy}i=-i\frac{\pi Q}{8w_0^2}\mathrm{csch}^2\left(\frac{\pi z}{2w_0}\right). \tag{18}$$

It is easily shown that the flow becomes uniform as $x\to\pm\infty$ ($\dot{u}_s-\dot{u}_y i=Q/4w_0$ as $x\to\pm\infty$), leading to vanishing strain rates. In fact, the flow becomes nearly uniform when the location under consideration, $x=h_0$, is several times larger than the width w_0. Figure 5 shows the variation of the normal velocity $\dot{u}_x$ at $x=\pm h_0$ across the width of the channel for different values of the ratio h_0/w_0. In this figure, $\dot{u}_x$ is normalized by $\dot{u}_0$, which is the normal velocity at $x=h_0$, $y=0$. It is seen that when the ratio of h_0/w_0 is unity, the maximum difference in $\dot{u}_x$ across the width is about 15 percent. When the ratio is 2.0, the maximum difference in $\dot{u}_x$ is only two percent, and $\dot{u}_x$ is approximately uniform across the width of the channel. In the following, we use the solution of the infinite channel to approximate the plastic flow field in the finite sized unit cell in Fig. 4.

The equilibrium condition can be satisfied in a weak form by using the principle of virtual work rate, as

$$2\int_{-w_0}^{w_0}\sigma_s\dot{u}_x^I dy=\int_V s_{ij}\dot{\varepsilon}_{ij}dV-2\int_{-w_0}^{w_0}\Delta T_i^I\dot{u}_i^I dy \tag{19}$$

where ΔT_i^I is the difference in traction at $x=\pm h_0$ between the average normal stress σ_s and the stress corresponding to the plastic flow, $\dot{u}_x^I$ and $\dot{u}_i^I$ are the displacement rates at $x=\pm h_0$ given in Eq. (17), and s_{ij}, $\dot{\varepsilon}_{ij}$ are the true deviatoric stress and true strain rate in the current configuration. Generally, when the ratio h_0/w_0 is sufficiently large (say, $\geqslant 1$), the contribution of the last term in Eq. (19) is negligibly small. In our numerical results, the contribution from this term is ignored.

Assuming that the material obeys the plastic stress-strain relation given in Eq. (1), and applying J_2-flow theory, we can obtain the relation of separation stress versus the displacement at $x=\pm h_0$ following the same steps as in Eq. (13) through Eq. (15), as

$$\frac{\sigma_s}{\sigma_Y}=\frac{1}{Q}\int_V f(\varepsilon_e)\dot{\varepsilon}_e dV. \tag{20}$$

The integration in Eq. (20) can be evaluated by a change of variables from Eulerian to Lagrangian coordinates, i.e., to the initial (undeformed) coordinates. The corresponding relations between the two sets of variables can be obtained by solving the differential equations in Eq. (17).

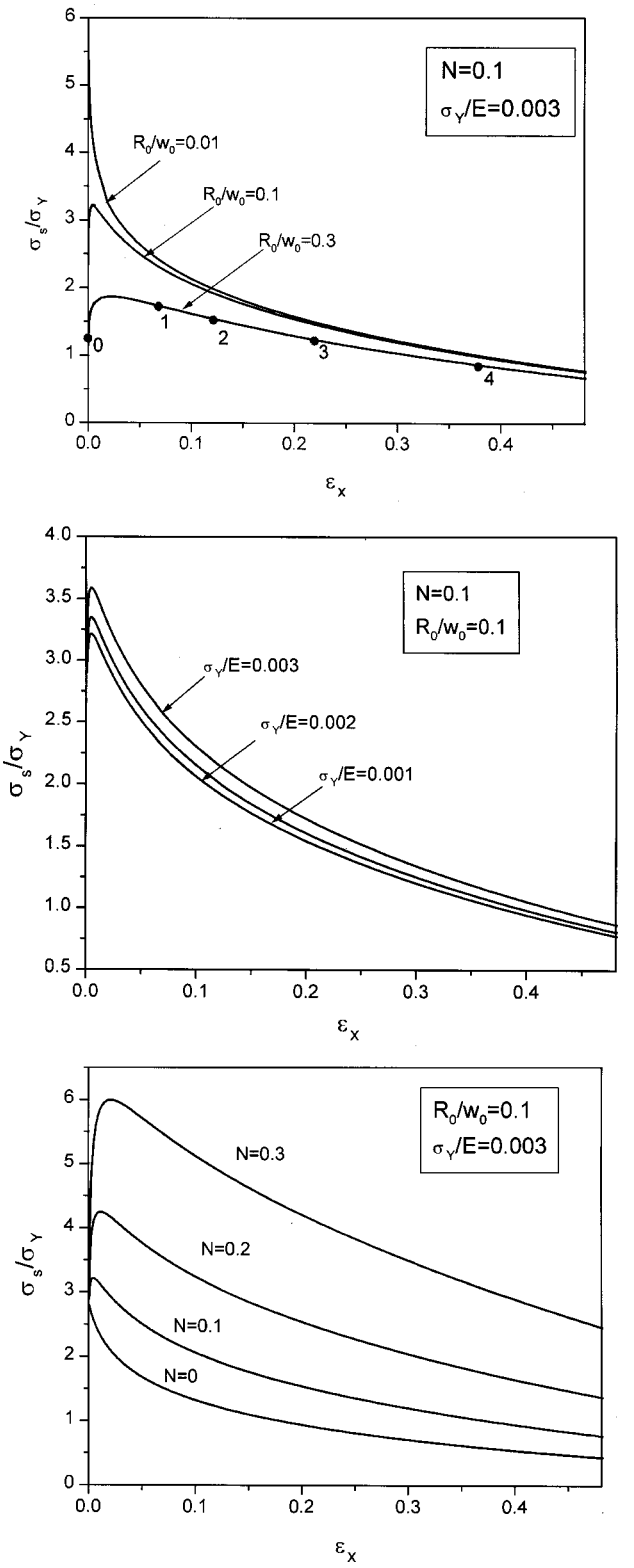

Fig. 6 Stress-separation relations for two-dimensional void growth; (*a*) effects of the initial radius of cavity, (*b*) effects of the material constant σ_Y/E, (*c*) effects of the strain-hardening exponent N

Results of the stress-separation curves are presented in Figs. 6(*a*)–(*c*). In these calculations, void spacing is taken to be the

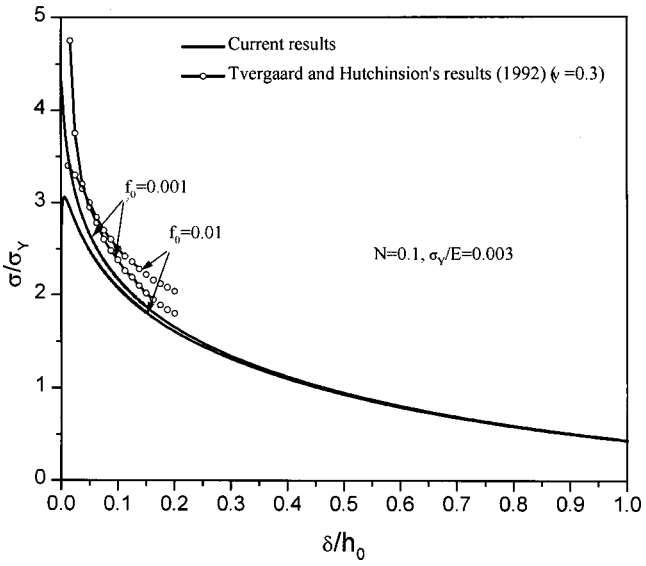

Fig. 7 Comparison of the stress-separation curves with Tvergaard and Hutchinson's calculations

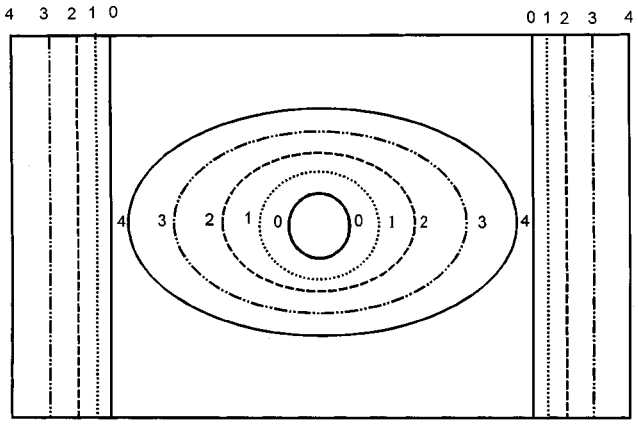

Fig. 8 Evolution of void shape for the two-dimensional case

same as the initial thickness of the layer, i.e., $h_0/w_0=1.0$. Figure 6(*a*) shows the separation stress normalized by the yield stress versus the average logarithmic strain of the cell, $\varepsilon_x=\ln(1+\delta/h_0)$, for different initial cavity size, a prescribed strain-hardening exponent N and normalized yield strength σ_Y/E. Figures 6(*b*) and (*c*) depict the effects of the material yield strength σ_Y/E and the strain-hardening exponent N on the stress-separation curves, respectively. The same trends as those in Fig. 2 are obtained. Figure 6(*a*) shows that, for small initial void size, peak separation stress (i.e., cavitation instability under the load-controlled loading condition) is reached rapidly at a very small strain level with a high maximum separation stress. For example, when $R_0/w_0=0.01$, $\sigma_s|_{\max}=5.45\sigma_Y$. On the other hand, larger initial void sizes result in lower peak stresses reached at much larger strains. The stress-separation curves decay monotonically beyond its peak stress as the void expands, leaving a narrow neck region between adjacent voids. Figures 6(*b*) and 6(*c*) again show that the stress separation curves are insensitive to σ_Y/E but rather sensitive to hardening exponent N.

Figure 7 shows the comparison of the stress-separation curves between the current result and that obtained by Tvergaard and Hutchinson [8] based on the Gurson model for elastoplastic material. Here f_0 is the area fraction of voids in the initial, undeformed state ($f_0=\pi R_0^2/4w_0h_0$), ν is Possion's ratio, δ is the separation displacement at the interface. All the parameters in our calculations are identical to those used by Tvergaard and Hutchinson [8] except for the Possion's ratio since there is no elastic deformation in our model. The Possion's ratio in Tvergaard and Hutchinson's calculation is 0.3 while in the current model it is 0.5 (rigid-plastic material). The absence of elastic deformation is likely the reason why the current model predicts a lower peak stress at a smaller displacement level and a somewhat lower separation stress than theirs, as shown in Fig. 7. Nevertheless, the two sets of curves in Fig. 7 exhibit general agreement. Due to the limitations of their finite element method, Tvergaard and Hutchinson terminated their calculations at a much lower separation displacement level than what we did using our model.

It is of interest to examine the shape evolution of cavities as they grow. Generally, an initially circular cavity becomes elliptical as it grows. Although the exact shape can be obtained by following the displacement of each material point on the boundary of the cavity, here we schematically depict the shape evolution by drawing an ellipse based on the long and short axes. Figure 8 shows an example of the evolution of the void shape under the prescribed parameters $R_0/w_0=0.3$, $N=0.1$, and $\sigma_Y/E=0.003$, where the numbers 0,1, . . . ,4 represent different instants of time during cavity growth. The corresponding instants are shown in Fig. 6(*a*). It is clear from Fig. 8 that, based on this model, the cavity mainly grows in the layer-thickness direction. This feature may be an artifact of the model since the mechanism of necking of ligaments is not accounted for.

4 Fracture Resistance

For purely brittle fracture of crystalline materials, the fracture toughness can be obtained by integrating the stress-separation curve at the atomic level. For a ductile material undergoing fracture due to plasticity induced cavitation, the fracture toughness can be evaluated by integrating an equivalent stress-separation curve, such as those obtained in the previous section, at a much larger length scale—the microscopic level. In this section we evaluate the fracture resistance of a sandwich structure exhibiting plasticity-induced cavitation in the thin ductile layer. Only the two-dimensional case will be considered in this section since the thickness of ductile layer and cavity spacing are ambiguously defined for the spherically symmetric cases.

The separation curves obtained in the previous sections are sensitive to the initial cavity size and to the hardening exponent, but they are nearly independent of the ratio of the yield strength to Young's modulus. Therefore, the effect of that ratio may be neglected. A universal expression of the stress-separation curve can be written as

$$\sigma_s(\delta)/\sigma_Y=F(N,V_f,G,\delta) \tag{21}$$

where N is the hardening exponent, δ is the separation displacement, V_f denotes the density of the voids along the interface, and G is a geometrical parameter related to the thickness of the ductile layer and the spacing between cavities. In the two-dimensional plane strain case, the initial density of cavities $V_f=R_0/w_0$, and the geometrical parameter G is the ratio of ductile layer thickness to the spacing between cavities h_0/w_0.

As pointed out by Tvergaard and Hutchinson [8,9], in evaluating the amplification of the fracture resistance due to plastic deformation, the work of separation per unit area (the initial separation resistance), Γ_0, and the ratio of peak separation stress to yield stress are two important parameters. The latter can be determined readily from the separation curves. The work of separation for the unit cell is

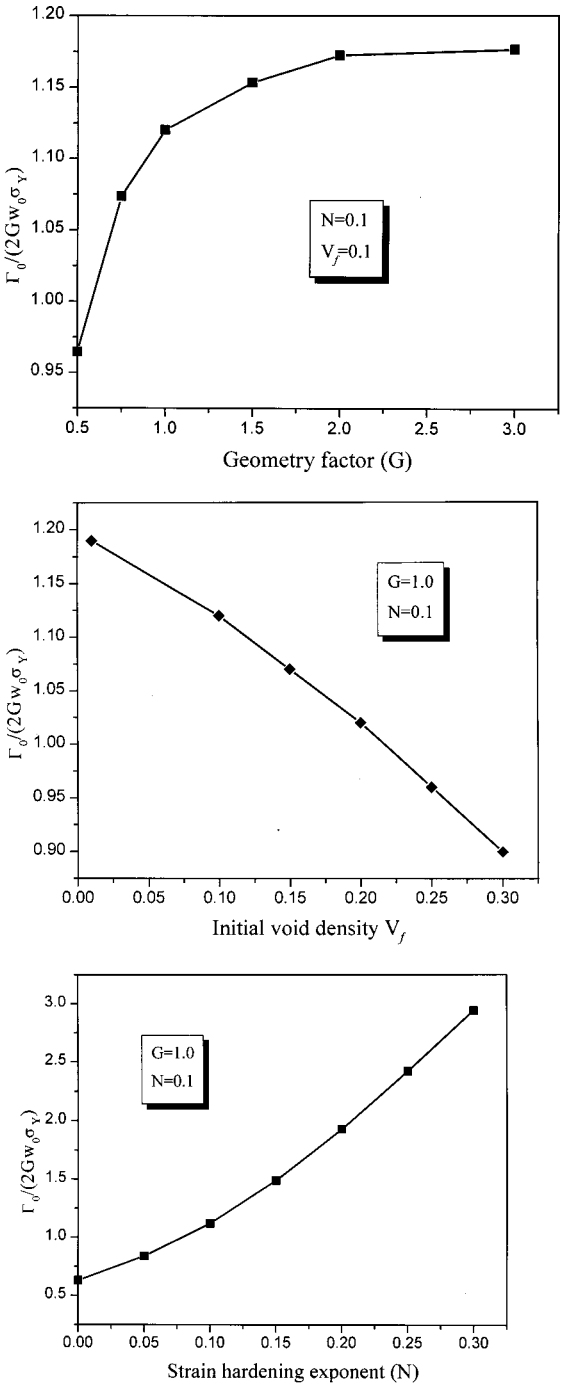

Fig. 9 (*a*) Normalized initial fracture resistance versus the geometrical parameter *G*, (*b*) normalized initial fracture resistance versus the void volume fraction V_f, (*c*) normalized initial fracture resistance versus the strain-hardening exponent *N*

$$W = 2\int_0^{U_1^*} T_s(\delta)\,d\delta \tag{22}$$

where U_1^* is the separation displacement level at which the total separation occurs ($\sigma_s \cong 0$), and T_s is the resultant force at the boundary of the cell. The initial separation resistance Γ_0 can then be expressed as

$$\Gamma_0 = W/A = 2\sigma_Y \int_0^{U_1^*} [\sigma_s(\delta)/\sigma_Y]\,d\delta \tag{23}$$

where the exposed surface area $A = 2w_0 t_0$, and t_0 is the thickness in the out-of-plane direction. In order to use the separation curves obtained in the previous section, Γ_0 may be rewritten as

$$\frac{\Gamma_0}{2w_0\sigma_Y} = G\int_0^{\varepsilon^*} [\sigma_s(\varepsilon)/\sigma_Y]\exp(\varepsilon)\,d\varepsilon \tag{24}$$

where ε^* denotes the true strain at the boundary of the unit cell corresponding to the displacement U_1^*. The functional form of $\sigma_s(\varepsilon)/\sigma_Y$ can be obtained from the stress-separation curves in the previous section. Since the separation curves are nearly independent of the material constant σ_Y/E, the normalized initial fracture resistance should then be nearly independent of σ_Y/E.

Equation (24) shows that the value of the normalized work of separation per unit area is determined by the integral on the right-hand side only. The integration can be carried out for given values of N, V_f, and G. The dependence of the normalized work of separation on the geometrical parameter, G, is shown in Fig. 9(*a*). For strain-hardening exponent $N = 0.1$ and the void density $V_f = 0.1$, the normalized initial fracture resistance $\Gamma_0/2w_0\sigma_Y$ has a rather weak dependence on $G(=h_0/w_0)$. The value of the normalized Γ_0 changes only from 0.95 to 1.17 when G varies from 0.5 to 3.0. Furthermore, when the value of G is larger than about 2.0, the normalized initial fracture resistance reaches an asymptotic value independent of G.

The dependence of the normalized fracture resistance $\Gamma_0/2w_0\sigma_Y$ on the hardening exponent and on the initial void density is shown in Figs. 9(*b*)–(*c*). They demonstrate that Γ_0 is very sensitive to the strain-hardening exponent, N, as shown in Fig. 9(*c*), but moderately sensitive to the void density, V_f, as shown in Fig. 9(*b*). For given void density V_f, as N changes from the nonhardening case ($N=0$) to a strong hardening case ($N=0.3$), the value of Γ_0 increases nearly sixfold. However, for given N, Γ_0 decreases moderately as V_f increases.

From Fig. 9(*a*)–(*c*) we can see that the value of the normalized Γ_0 for the two-dimensional case is in the range of 0.5–1.75 for $N=0-0.2$. This is higher than the values (0.35–0.82) predicted by Tvergaard and Hutchinson [8]. Tvergaard and Hutchinson abruptly terminated their calculations when the void area fraction equals 0.2, and neglected the contribution of the stress-separation curve beyond that point. This undoubtedly results in a lower work of fracture than that predicted by our calculations.

5 Concluding Remarks

In the present paper, we have developed a new technique to solve solid mechanics problems involving large plastic deformation for which closed-form solutions are difficult or sometimes impossible to obtain. The technique involves using the fluid flow field from existing fluid mechanics solutions to approximate the plastic flow field, and using the principle of virtual work to satisfy the equilibrium condition. It should be pointed out that the major difference between flow of fluids and plastic flow of solids is the following: In the potential flow of fluids, there is no shear stress; whereas in plastic flow of solids, the shear stress (the Mises equivalent stress in the present model) is constant for nonhardening materials or nearly constant for weakly hardening materials. In general, the method we developed here may be applied to a variety of solid mechanics problems, as long as the fluid mechanics solution is readily available.

This technique is used here to address a particular mechanism of interfacial fracture—cavitation in a thin ductile layer in a sandwich structure. Although this problem may be solved using numerical methods, as has indeed been done by Tvergaard [14] using the finite element method, the method developed here has the clear advantage when carrying out a parametric study involving extremely large deformation. Solving the two-dimensional cavity growth problem using the present method is much less time-consuming compared to, e.g., that using the finite element method with remeshing.

Two configurations have been considered in this paper: a spherically symmetric case for which a closed-form solid mechanics solution exists; and a two-dimensional, plane strain problem for which no closed form solution exists. In both cases, the potential fluid flow field from a point source is used to approximate the plastic deformation field surrounding the growing cavity in a representative unit cell. The current method gives the exact solution for the spherically symmetric cavity growth problem. For the two-dimensional plane strain cavity growth problem, reliable stress-separation relations have been obtained. The results show that the initial size of the void and the strain-hardening exponent are two important parameters that strongly affect the stress-separation curves. The stress-separation relations are also dependent on such geometrical parameters as the layer thickness and the void spacing. The interfacial fracture resistance due to this mechanism, evaluated by integrating the stress-separation curves, is strongly dependent on the strain-hardening exponent, is moderately dependent on cavity density, and is nearly independent on the geometrical parameter G.

In the present paper, void coalescence due to the necking of ligaments is not addressed. The interaction between adjacent voids is modeled by simply specifying the Neumann boundary conditions for each representative unit cell, i.e., the normal displacement at the boundaries of the unit cell between adjacent voids vanishes. Therefore the model is not accurate when necking instability and coalescence take place between adjacent voids. Furthermore, necking would result in accelerated separation of the fracture planes, leading to a rapid load drop in the stress-separation curves. Hence the final stage of the stress-separation curves predicted by the present model may not be very accurate. Fortunately, this stage of the separation process has only insignificant contributions to the overall fracture resistance.

There are several implications of the results by the present model. As shown in Fig. 9, as the void density increases, i.e., as the spacing between voids decreases, the fracture resistance decreases monotonically. This result implies that, in an adhesively bonded structure, a finer interfacial microstructure with more densely distributed void nucleation sites will give rise to a lower interfacial fracture toughness. However, a finer microstructure also means a smaller initial cavity size; thus it requires a higher peak stress to reach instability during void growth. Therefore, there could exist a preferred combination of pore size and pore spacing of the interfacial microstructure that will result in an optimal performance of the sandwich structure. Identification of such optimal combination will provide guiding principles for preparing the surfaces of structural components (e.g., aluminum panels) for adhesive bonding.

Acknowledgment

The work has been supported by the U. S. Department of Energy through Grant No. DEFG02-96ER45607. The authors are grateful for helpful discussions with Prof. H. Aref.

References

[1] Bowlin, D. T., Scheeline, A., and Pearlstein, A. J., 1997, ''Current Oscillations in Potentiostatic Electro-Oxidation of Aluminum in Sulfuric and Phosphoric Acids,'' Electrochim. Acta, **43**, pp. 417–421.
[2] Gao, H., Scheeline, A., and Pearlstein, A. J., 1999, ''Demonstration of a Novel Rotating Cylindrical Electrode in Growth of Oxide Films With Spatially Controlled Microstructural Variation on Al 6061,'' *Proceedings of the International Symposium on New Directions in Electroanalytical Chemistry II*, 1999, J. Leddy, P. Vanysek, and M. D. Porter, eds., The Electrochemical Society, Pennington, NJ, pp. 109–115.
[3] Ashby, M. F., Blunt, F. J., and Bannister, M., 1989, ''Flow Characteristics of Highly Constrained Metal Wires,'' Acta Metall., **37**, pp. 1847–1857.
[4] Evans, A. G., and Dalgleish, B. J., 1992, ''The Fracture Resistance of Metal-Ceramic Interfaces,'' Acta Metall. Mater., **40**, Suppl., pp. S295–S306.
[5] Turner, M. R., Dalgleish, B. J., He, M. Y., and Evans, A. G., 1995, ''A Fracture Resistance Measurement Method for Bimaterial Interfaces Having Large Debond Energy,'' Acta Metall. Mater., **43**, pp. 3459–3465.
[6] Turner, M. R., and Evans, A. G., 1996, ''An Experimental Study of the Mechanisms of Crack Extension Along an Oxide/Metal Interface,'' Acta Mater., **44**, pp. 863–871.
[7] He, M. Y., Evans, A. G., and Hutchinson, J. W., 1996, ''Interface Cracking Phenomena in Constrained Metal Layers,'' Acta Mater., **44**, pp. 2963–2971.
[8] Tvergaard, V., and Hutchinson, J. W., 1992, ''The Relation Between Crack Growth Resistance and Fracture Process Parameters in Elastic-Plastic Solids,'' J. Mech. Phys. Solids, **40**, pp. 1377–1397.
[9] Tvergaard, V., and Hutchinson, J. W., 1996, ''Effect of Strain-Dependent Cohesive Zone Model on Predictions of Crack Growth Resistance,'' Int. J. Solids Struct., **33**, pp. 3297–3308.
[10] McClintock, F. A., 1968, ''A Criterion for Ductile Fracture by the Growth of Holes,'' ASME J. Appl. Mech., **35**, pp. 363–371.
[11] Rice, J. R., and Tracey, D. M., 1969, ''On the Ductile Enlargement of Voids in Triaxial Stress Fields,'' J. Mech. Phys. Solids, **17**, pp. 201–217.
[12] Needleman, A., 1972, ''Void Growth in an Elastic-Plastic Medium,'' ASME J. Appl. Mech., **39**, pp. 964–970.
[13] Andersson, H., 1977, ''Analysis of a Model for Void Growth and Coalescence Ahead of a Moving Crack Tip,'' J. Mech. Phys. Solids, **25**, pp. 217–233.
[14] Tvergaard, V., 1997, ''Studies of Void Growth in a Thin Ductile Layer Between Ceramics,'' Comput. Mech., **20**, pp. 186–191.
[15] Huang, Y., Hu, K. X., Yeh, C. P., Li, N.-Y., and Hwang, K. C., 1996, ''A Model Study of Thermal Stress-Induced Voiding in Electronic Packages,'' ASME J. Electron. Packag., **118**, pp. 229–234.
[16] Huang, Y., Hutchinson, J. W., and Tvergaard, V., 1991, ''Cavitation Instabilities in Elastic-Plastic Solids,'' J. Mech. Phys. Solids, **39**, pp. 223–241.
[17] Tvergaard, V., and Hutchinson, J. W., 1993, ''Effect of Initial Void Shape on the Occurrence of Cavitation Instabilities in Elastic-Plastic Solids,'' ASME J. Appl. Mech., **60**, pp. 807–812.
[18] Hou, H.-S., and Abeyaratne, R., 1992, ''Cavitation in Elastic and Elastic-Plastic Solids,'' J. Mech. Phys. Solids, **40**, pp. 571–592.